



Influence of Dynamic Disturbance on the Creep of Sandstone: An Experimental Study

Wancheng Zhu¹ · Shaohua Li¹ · Shuai Li¹ · Leilei Niu¹

Received: 30 April 2018 / Accepted: 28 October 2018 / Published online: 2 November 2018
© Springer-Verlag GmbH Austria, part of Springer Nature 2018

Abstract

Dynamic disturbance such as blasting may significantly affect the creep of rock. Quantification of the influence of dynamic disturbance on the creep behavior of rock is a prerequisite to the understanding of the long-term behavior of rock around excavations. In this study, a new creep-impact test machine that is capable of testing the rock failure behavior under combined creep loading and dynamic disturbance was introduced. We performed creep experiments on sandstone while a dynamic disturbance was applied. Axial strain, volumetric strain and acoustic emission (AE) events were measured. The results from the creep-impact experiment show that the rock creep was greatly affected by the dynamic disturbance. Dynamic disturbance may introduce further damage on rock and shorten the time-to-failure of creeping rock specimens. Combination of creep stress and dynamic disturbance resulted in two failure conditions: failure along with accelerating creep and failure during dynamic disturbance. If the dynamic disturbance was not followed by failure, the axial strain consisted of an instantaneous response as the dynamic disturbance was applied, followed by a primary phase of decelerating creep and a steady-state creep phase. This pattern was repeated after the next dynamic disturbance until the last dynamic disturbance that led to the failure. The creep resulted from micro-fracturing in the rock, which can be characterized by the cumulative AE energy if the AE events were monitored during the creep-impact test of rock. The creep behavior was more sensitive to dynamic disturbance under higher creep stress. Under the same creep stress, a dynamic disturbance with higher impact energy resulted in a higher axial strain rate, absolute volumetric strain rate and AE energy rate. Dynamic disturbance not only increased the axial strain rate but also promoted the dilatancy of the rock specimens. The failure of the rock specimens was mostly in the shear mode, and this failure pattern was merely affected by the dynamic disturbance, even though the specimens became more fragmented under the higher creep stress and higher impact energy.

Keywords Rock creep · Creep-impact experiment · Dynamic disturbance · Acoustic emission (AE) · Accelerating creep

List of Symbols

D	Diameter of hammer (mm)
R	Curvature radius of hammer (mm)
L	Length of hammer (mm)
ϵ_v	Volumetric strains of the rock specimen
ϵ_a	Axial strains of the rock specimen measured by strain gauge
ϵ_l	Circumferential strains of the rock specimen measured by strain gauge

t	Time (hours)
σ_p	Uniaxial compressive strength

1 Introduction

The creep properties of rock are not only of fundamental importance in the design of pillars (Obert 1965) and mining rooms (Dawson and Munson 1983) but also crucial for predicting the long-term evolution of rock engineering (Urai et al. 1986; Mortazavi and Molladavoodi 2012). Rock can deform nonlinearly over extended period of time and fail under creep stress well below the short-term failure strength (Heap et al. 2009a). Such time-dependent deformation of brittle rock at constant stress is termed brittle creep (Heap et al. 2011; Brantut et al. 2013), a process leading to delayed failure (Kranz et al. 1982; Brantut

✉ Wancheng Zhu
zhuwancheng@mail.neu.edu.cn

¹ Center for Rock Instability and Seismicity Research, Department of Mining Engineering, School of Resource and Civil Engineering, Northeastern University, 110819 Shenyang, China

et al. 2012, 2013). In brittle creep, macroscopic failure is preceded by accelerating deformation.

In early 1939, Griggs (1939) conducted creep studies on rock and concluded that rock can deform with time as the constant stress reaches a certain proportion of the short-term failure strength. Over the past decades, creep behavior has been extensively investigated in many rock types, such as rock salt (Hansen 1978), granite (Fujii et al. 1999; Chen et al. 2015; Xu et al. 2017), sandstone (Baud and Meredith 1997; Heap et al. 2009a; Ngwenya et al. 2001; Brantut et al. 2014a), tuff (Ma and Daemen 2006; Ye et al. 2015), limestone (Brantut et al. 2014b; Nicolas et al. 2017) and shale (Sone and Zoback 2014). Brittle creep deformation is an important characteristic of rock (Brantut et al. 2013; Aydan et al. 2014). Existing data (Main 2000; Brantut et al. 2013; Nicolas et al. 2017) show that brittle creep deformation exhibits three stages of behavior: (1) decelerating creep, (2) steady creep, and (3) accelerating creep. The cumulative number of acoustic emissions (AE) and cumulative AE energy were observed to qualitatively follow the same tri-modal behavior as the strain (Lockner and Byerlee 1977; Baud and Meredith 1997). The majority of studies focused on the influence of the differential stress (Fujii et al. 1999; Heap et al. 2011; Brantut et al. 2012), effective pressure (Kranz 1980), temperature (Kranz et al. 1982; Niemeijer et al. 2002; Heap et al. 2009b) and initial porosity (Ngwenya et al. 2001; Brantut et al. 2013) on brittle creep behavior.

Many theoretical analyses have also been conducted. Empirical models using a logarithmic function, a power function and other differential equations (Molladavoodi and Mortazavi 2011; Zhang et al. 2012; Chen et al. 2014) were defined to reproduce the brittle creep behavior. Yoshida and Horii (1992) proposed a micromechanical model for brittle creep to analyze the creep behavior of underground structures. Brantut et al. (2012) developed a micromechanical model to describe time-dependent brittle creep of water-saturated rock under triaxial stress condition, where the brittle creep was explained by subcritical crack growth that mainly resulted from stress corrosion (Anderson and Grew 1977; Atkinson 1984; Atkinson and Meredith 1987; Costin 1987).

However, rock masses are not necessarily under a constant-stress condition (Zhu et al. 2016). During mining, rock masses are exposed to dynamic disturbance, such as blasting (Zhu et al. 2010). Thus, most rock masses are under a combined static, creep and dynamic stress condition (Li et al. 2008). The dynamic disturbances may play a crucial role in triggering rock burst in underground engineering (Wang and Huang 1998; Mansurov 2001), although the high elastic energy stored in the rock mass is a prerequisite for rock burst occurrence. For instance, approximately 75% of rock bursts occur with, or in the hour following a blasting activity (Whyatt et al. 2002). Detailed knowledge of the effect of

dynamic disturbance on rock creep is a vital prerequisite for understanding the long-term response of rock.

A few studies have shed light on the influence of dynamic disturbance on creep behavior. Malan et al. (1997) and Malan (1999) monitored the creep deformation in mining practices during blasting. Their results showed that there is an instantaneous closure at blasting time, followed by a primary phase of decelerating closure within hours, then a steady-state closure phase until the next blast occurs, and this pattern repeats. In a laboratory-based, real-time computerized tomography (CT) study, Fu et al. (2008) studied the micro-damage evolution of gray-green mudstone during creep disturbed by dynamic impact and concluded that the response of rock to the dynamic disturbance is generally controlled by the stress proximity to the rock strength. Despite these studies, there is still much to learn about the influence of dynamic disturbance on creep of rock. Our understanding of the influence of dynamic disturbance on tertiary creep remains embryonic, although some effort has been made. Therefore, it is very significant to perform creep experiments on sandstone while dynamic disturbance is applied, to clarify the rock failure mechanism under combined creep and dynamic loading.

In this paper, we introduce a creep-impact test machine to measure the effect of dynamic disturbance on creep. First, a series of conventional brittle creep experiments were conducted as the basis of creep-impact experiments of sandstone. Then, creep-impact experiments, together with AE monitoring, were performed to investigate the effect of dynamic disturbance on creep. Finally, the effect of creep stress and impact energy on the creep deformation and failure of rock is discussed.

2 The Rock Creep-Impact Test Machine and Experimental Methodology

2.1 Rock Creep-Impact Test Machine

The rock creep-impact test machine consists of three key components: constant-stress loading system, dynamic-disturbance loading system, and data acquisition and recording system (Fig. 1). The long-term constant-stress condition was maintained using a hydraulic control method. The maximum creep loading of this equipment is 400 kN. Dynamic disturbance was generated by a falling hammer when it impacts the incident steel bar, as shown in Fig. 2. The hammer is raised to the specified height, and it is released to fall along two steel columns and impacts the incident steel bar that is in contact with the rock specimen; thus, the dynamic disturbance is applied on the rock specimen that may be during creep deformation. The diameter and length of the steel columns are 20 mm and 2000 mm, respectively. In this respect,

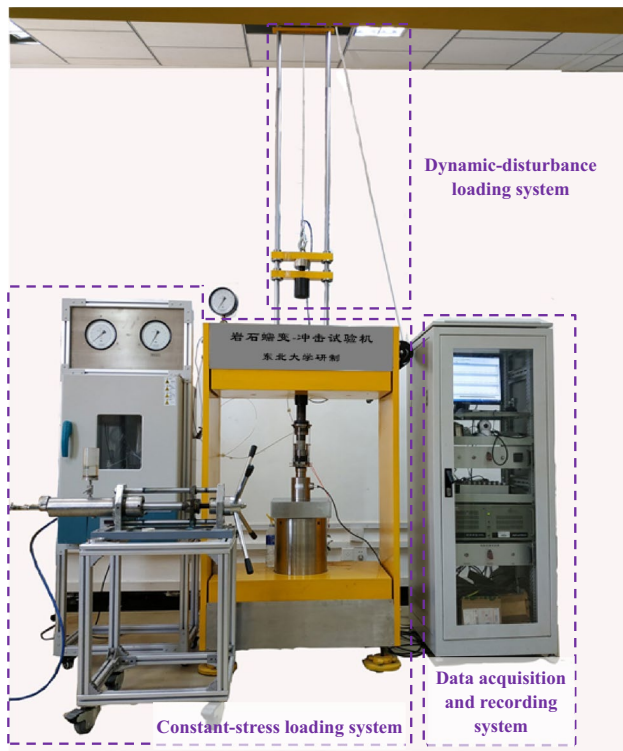


Fig. 1 Photograph of the rock creep-impact test machine

the maximum falling height of the hammer is 2000 mm, and the dynamic stress generated is controlled by the weight and the falling height of the hammer.

Based on previous experiences with the design of the hammer (Zhu et al. 2015), a falling hammer with a cambered impact surface was made (Fig. 2c). Introducing a cambered surface as the impactor was expected to produce a gradual building-up of the incident stress wave, thus increasing the wave-rise duration (Li et al. 2017, 2018), which was essential to achieve stress uniformity in the rock specimen (Zhang and

Zhao 2014). The weight of the hammer was 5.0 kg. As shown in Fig. 2, the diameter (D) was 80 mm, the curvature radius (R) was 100 mm and the length (L) was 126.7 mm.

During the creep phase, the axial creep stress was recorded with a load cell below the specimen, and creep strain was recorded with strain gauges attached on the surface of the rock specimen. All signals were recorded by a digital oscilloscope (DL750 ScopeCorder, Yokogawa Electric Corp., Tokyo, Japan), and the data were stored on a PC. To understand the deformation mechanism of the rock specimen subjected to creep-impact loading, AE events were monitored continuously via six Nano30 piezoelectric transducers mounted on the rock specimens and stored by a PAC PCI-II acoustic emission system. The threshold was set at 45 dB to gain a high signal/noise ratio. The sampling frequency was set at 5 MHz. The positions of the six AE transducers are shown in Fig. 3. It was noted that the high-level noises generated by the impact were unavoidably mixed with the actual AE signals during the dynamic disturbance; therefore, it was difficult to distinguish the real AE events from the background noise. Additionally, because the experiment’s focus was to study the influence of dynamic disturbance on the creep behavior, the AE signals during the dynamic disturbance were not recorded.

Once the desired creep stress was achieved, dynamic disturbance was applied using a falling hammer. The incident stress wave was recorded by the strain gauges attached on the steel bar above the rock specimen. Strain gauges in an axial and circumferential configuration were wired into a full Wheatstone bridge circuit with a dummy specimen and were used to monitor principal strain development. The resistance of strain gauges used for static strain is 120 Ω . The volumetric strain ϵ_v can be calculated using the following formula:

$$\epsilon_v = \epsilon_a + 2\epsilon_l, \tag{1}$$

where ϵ_a is axial strain and ϵ_l is lateral strain. Once the dynamic disturbance is applied, an incident stress wave is

Fig. 2 Dynamic disturbance loading system and design of hammer. **a** Photo of the dynamic disturbance loading system. **b** The application of dynamic disturbance on rock specimen. **c** Hammer with cambered surface, D Diameter of the hammer, L Length of the hammer, R Curvature radius of cambered surface of the hammer

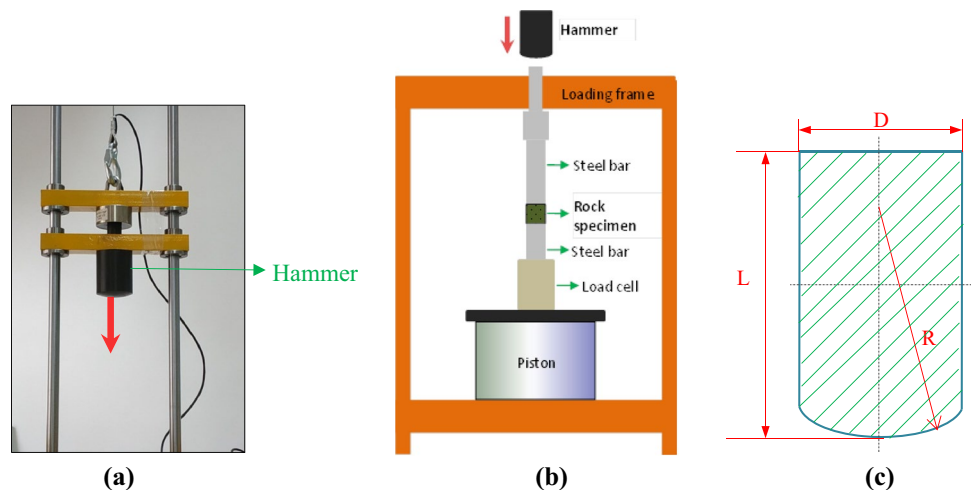


Fig. 3 Layout of the transducers for monitoring acoustic emission (AE) events of the rock. Specimens: **a** three-dimensional position of the six piezoelectric transducers on rock specimen; **b** angular position of the six piezoelectric transducers on the rock specimen

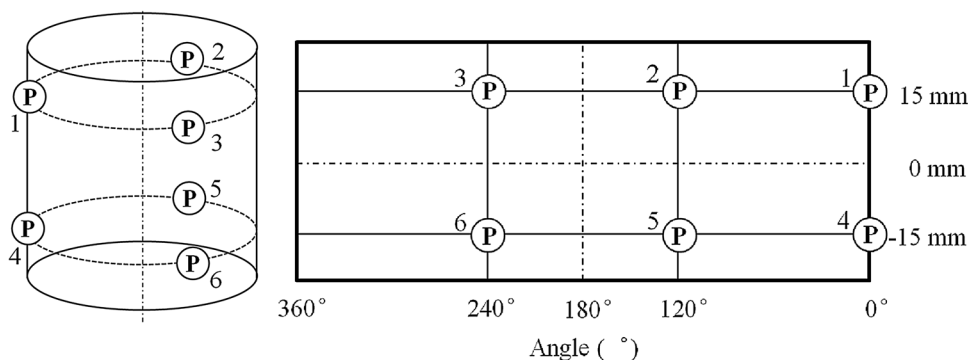


Table 1 Mineral composition and physical–mechanical parameters of the sandstone

Parameters	Values
Mineral composition	60% quartz, 20% feldspar, 15% kaoline, 5% mica
Grain size (mm)	0.2–0.5
Uniaxial compressive strength (MPa)	33.16
Tensile strength (MPa)	2.27
Elasticity modulus (GPa)	8.4
Poisson's ratio	0.29
Cohesion (MPa)	5.92
Internal friction angle (°)	27.39
Density ($\text{g} \cdot \text{cm}^{-3}$)	2.17
Porosity	$4.5 \pm 0.5\%$
Mean <i>P</i> -wave velocity (m s^{-1})	2630

excited on the top of the rock specimen, and it travels back and forth in the specimen because of wave transmission and reflection caused by difference between the impedance of the steel bars and the rock specimen.

2.2 Specimen Material and Preparation

The material used throughout this study was sandstone (Neijiang Municipality, China). To allow the results to be compared, the sandstone specimens used in this study were cored from a single block without distinct layering or lamination. The rock consists of 60% quartz, 20% feldspar, 15% kaolinite, and 5% mica. The grain size of the sandstone varies from 200 to 500 μm . The composition and physical properties of the sandstone are summarized in Table 1. The *P*-wave velocity was 2630 m/s for specimens of sandstone. The specimens were precision ground to a strict tolerance of ± 0.02 mm, and the travel time of the stress wave along the rock specimen axis was ~ 18.2 μs .

We monitored the strain with strain gauges attached on the rock specimen during the entire loading process. We calculated the strain of the whole rock specimen by the

strain value of the small area where the strain gauges were located. When this strain was used to represent the strain of the whole rock specimen, the uniformity of the stress in the rock specimen was the precondition. In this regard, according to Xia and Yao (2015) and Aben et al. (2016), a rock specimen with the length to diameter of 1:1 facilitates meeting the requirement of stress uniformity.

3 Experimental Methodology

Prior to performing creep experiments, quasi-static tests at a strain rate of $1.0 \times 10^{-5} \text{ s}^{-1}$ were conducted to obtain the stress–strain curves of the sandstone. A representative stress–strain curve is shown in Fig. 4. The peak strength of the sandstone was 33.11 MPa. As shown in Fig. 4, point C' marked the onset of dilatant cracking as the stress becomes high enough to initiate the growth of primarily axial micro-cracks (Brace et al. 1966). Beyond point C', the volumetric strain reached the maximum at point D', which marked the transition from compaction-dominated to dilatancy-dominated deformation because of increased dilatant cracking (Heap et al. 2009a). According to Baud and Meredith (1997), the level of creep stress should be higher than that at point C', corresponding to the onset of dilatancy, but lower than the stress level under which the rock specimen will fail within a few seconds or a few minutes. In this study, the constant creep stress was selected to be 19.86 MPa, 23.18 MPa and 26.49 MPa, corresponding to the stress level at 60%, 70% and 80% of the uniaxial compressive strength of 33.11 MPa, respectively.

To study the influence of impact energy on the failure of creeping rock specimens, the falling heights of the falling hammer were selected as 300 mm, 400 mm and 500 mm, and the corresponding impact energies were 14.7 J, 19.6 J and 24.5 J, respectively. During the impact of the dropping hammer, the overall stress applied on the rock specimen was not a constant but a variable, as shown in Fig. 5a, until it returned to the creep stress after approximately 20,000 μs . In this regard, the overall stress applied on the rock specimen

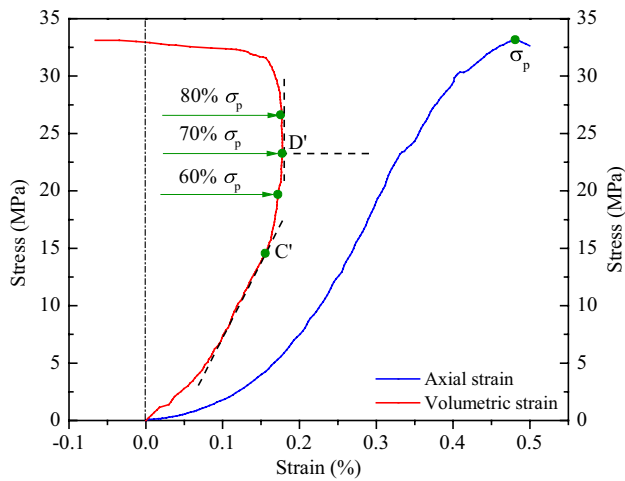


Fig. 4 Representative stress–strain curve of the rock specimens under uniaxial compression. C' marks the stress at which the onset of dilatant cracking microcracks occurs; D' marks the stress at which a dilatancy-dominated deformation occurs; σ_p marks short-term peak stress. The stress levels for conventional creep experiment and creep-disturbance experiment are indicated

was the superposition of creep stress and dynamic stress, the dynamic disturbance may alter the creep stress, but the specimen would restore to the same creep stress after a while.

All of the rising times of the generated stress waves (Fig. 5b) were more than 150 μs , which was sufficiently long to achieve stress uniformity in the rock specimen. The corresponding peak stresses of the incident dynamic stress were 20.12 MPa, 27.43 MPa and 33.46 MPa. The corresponding loading rates of the incident stress were 0.154 MPa/ μs , 0.172 MPa/ μs and 0.246 MPa/ μs .

As shown in Fig. 6, the first dynamic disturbance was performed after 12 h and the remaining dynamic disturbances were performed at 12-h intervals until the specimen failed.

Figure 7 shows the dynamic forces on the top and bottom ends of the rock specimen disturbed by the hammer with impact energy of 14.7 J. The dynamic force on the bottom end of the rock specimen was $\sim 20 \mu\text{s}$ later than the dynamic force on the top end, which resulted from the transmission of the dynamic stress wave across the rock specimen. However, throughout the process of impact, the dynamic force on the top end equaled that on the bottom end, which means that the balance of dynamic forces on both ends of the rock specimen was achieved.

4 Experimental Results

4.1 Conventional Creep Experiments

In the conventional creep experiments, the sandstone was first loaded to the predetermined stress level at a constant

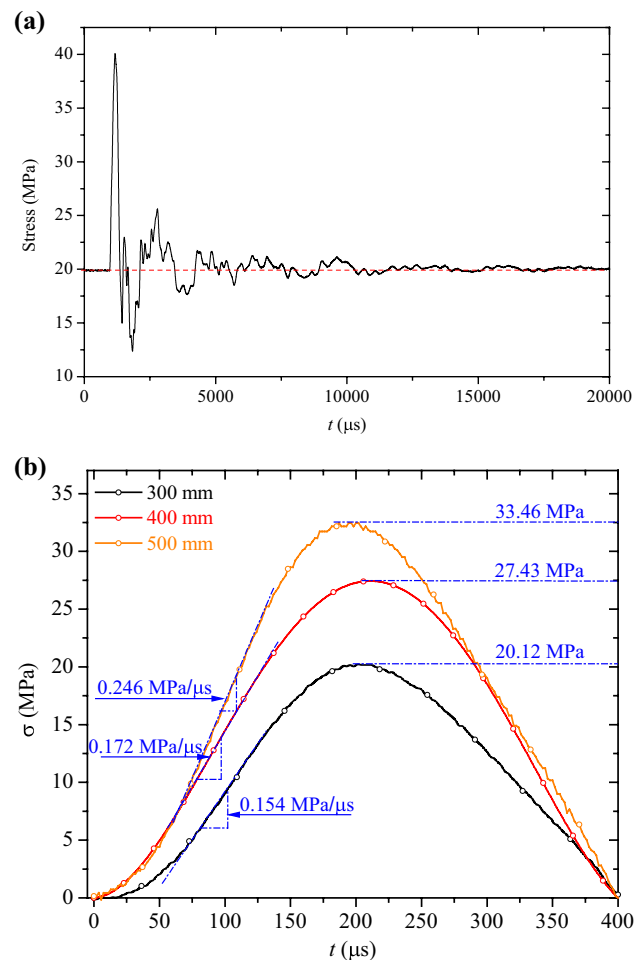


Fig. 5 Dynamic disturbance generated by the falling hammer. **a** Stress variation with time during impact; **b** incident stress waves generated by the hammer falling from heights of 300, 400 and 500 mm. The peak stress and the loading rate are indicated

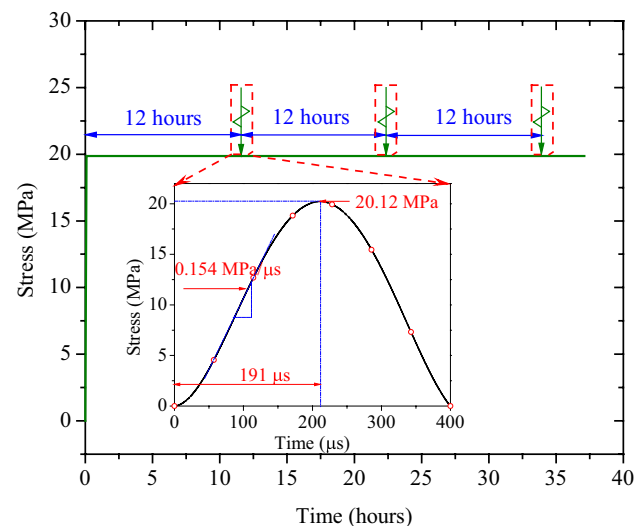


Fig. 6 Loading path during the creep-impact experiment of the rock specimen. The time for applying dynamic disturbances is indicated

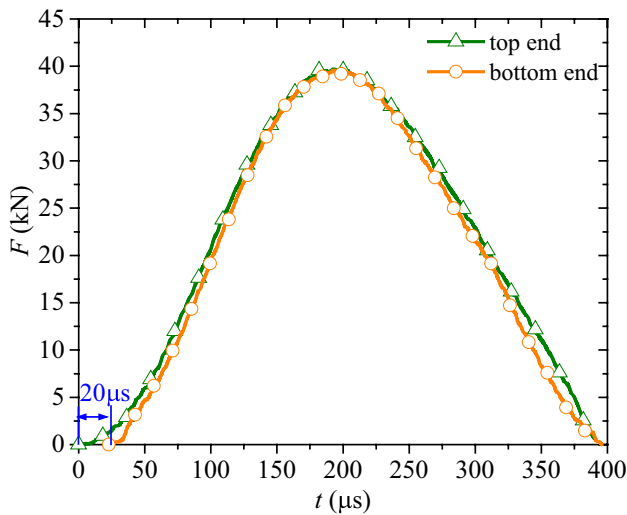


Fig. 7 Dynamic forces on the top and bottom ends of the rock specimens during the dynamic disturbance

stress rate of 5 MPa/min. Then, the loading stress was maintained constant, and the rock specimen was allowed to deform for 40 h or until failure. As shown in Fig. 8, under the stress of 19.86 MPa and 23.17 MPa, both the axial strain and the volumetric strain were characterized by an initially high strain rate that decreased to reach a quasi-linear steady creep. During the steady-state creep, the axial strain rates were $7.6 \times 10^{-10} \text{ s}^{-1}$ and $2.5 \times 10^{-10} \text{ s}^{-1}$, and the corresponding volumetric strain rates were $4.3 \times 10^{-10} \text{ s}^{-1}$ and $-2.9 \times 10^{-10} \text{ s}^{-1}$. Under the creep stress of 26.48 MPa, both the axial strain curve and the volumetric curve exhibited three stages of behavior before the specimen failed at 33.33 h.

4.2 Time-To-Failure during Creep-Impact Experiments

A summary of the time-to-failure during the creep-impact experiments is listed in Table 2. Under the combined creep loading and dynamic disturbance, rock specimens failed with two possible conditions: failure with accelerating creep and failure during dynamic disturbance. Figure 9 shows the total time-to-failure of rock specimens under different creep stress and impact energy. Comparing the results with those under conventional creep, the time-to-failure of rocks during the creep-impact experiment was shortened significantly with increasing creep stress. Moreover, the time-to-failure also shortened with increasing impact energy under the same creep stress except for the creep stress of 26.48 MPa. When we zoomed in on the experimental points under the creep stress of 26.48 MPa, it was found that the times-to-failure of rock specimens under this creep stress were almost the same. This indicated that the dynamic disturbance may accelerate

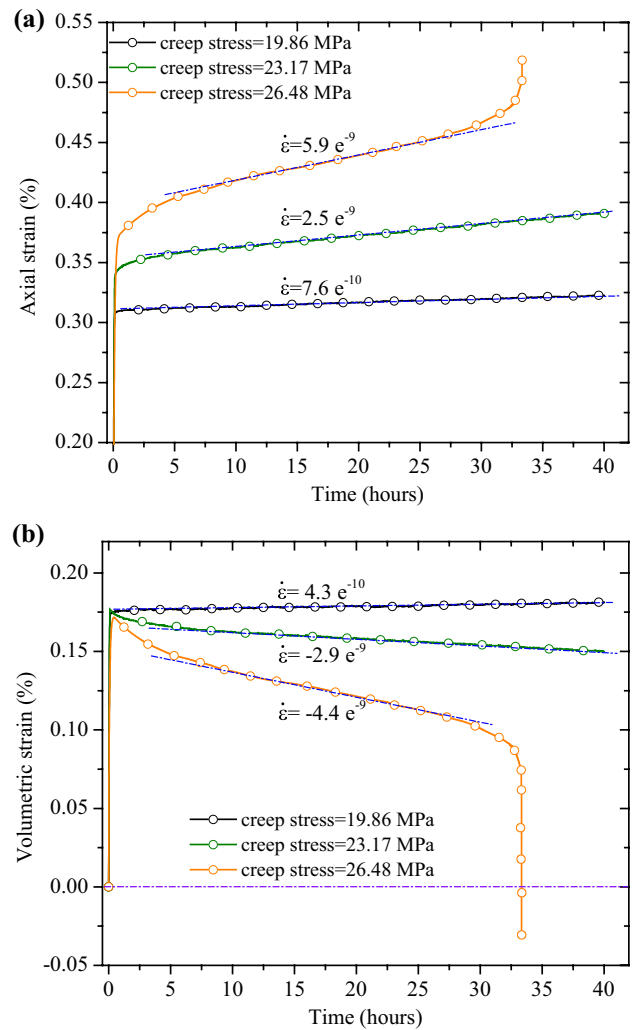


Fig. 8 Strain–time curves during conventional creep experiment conducted at different creep stresses: **a** axial strain, **b** volumetric strain. The axial strain rate and the volumetric strain rate are indicated in the figure

the failure of rock creep only when the rock was under sufficiently high creep stress.

4.3 Influence of Dynamic Disturbance on Creep

4.3.1 Typical Strain Curves During Creep-Impact Experiments

The deformation and failure of specimens under the creep stress of 19.86 MPa and dynamic disturbance with impact energy of 14.7 J is described as an example to illustrate the creep behavior of the rock specimen. As shown in Fig. 10a, the axial strain was obviously affected by the first and second dynamic disturbances, as there was a sudden increase in the axial strain during the dynamic disturbance and a primary decelerating phase followed by a steady-state phase.

Table 2 Summary of time-to-failure of rock specimens during creep-impact experiments

Creep stress (MPa)	Impact energy (J)	Count of dynamic disturbance	Total time-to-failure (h)	Time-to-failure after last dynamic disturbance (h)	Failure type
19.86	14.7	3	37.26	1.26	Accelerating creep
19.86	19.6	2	33.68	9.68	Accelerating creep
19.86	24.5	2	28.2	4.2	Accelerating creep
23.17	14.7	2	24	0	Failure during dynamic disturbance
23.17	19.6	1	20.09	8.09	Accelerating creep
23.17	24.5	1	14.94	2.94	Accelerating creep
26.48	14.7	1	12.42	0.42	Accelerating creep
26.48	19.6	1	12	0	Failure during dynamic disturbance
26.48	24.5	1	12	0	Failure during dynamic disturbance

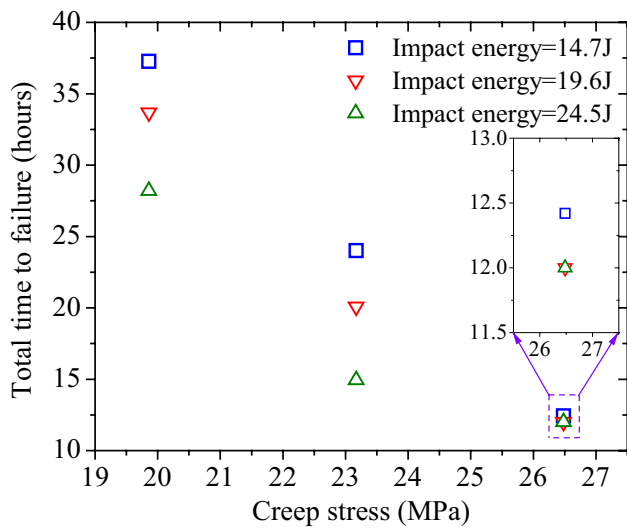


Fig. 9 Total time-to-failure of the rock specimens under different creep stresses and impact energies

Moreover, it is worth noting that under this condition of creep stress and impact energy, the rock specimen did not fail instantaneously during the third dynamic disturbance. Instead, after the third dynamic disturbance, the rock specimen deformed further and failed at $t = 37.27$ h, characterized as accelerating creep. In comparison with the rock specimen under the conventional creep, the dynamic disturbance increased the axial strain rate and facilitated the accelerating creep, which reflects the failure mechanism triggered by the dynamic disturbance.

The volumetric strain curve during the creep-impact experiment is shown in Fig. 10b. Affected by the first dynamic disturbance, the volumetric strain showed a sudden increase, but the volumetric strain then showed a tendency to decrease during most of the 12–24-h period. Due to the second dynamic disturbance, there was a sudden decrease in the volumetric strain rate; then, a more gradual steady-state volumetric strain rate followed. Finally, the rock specimen

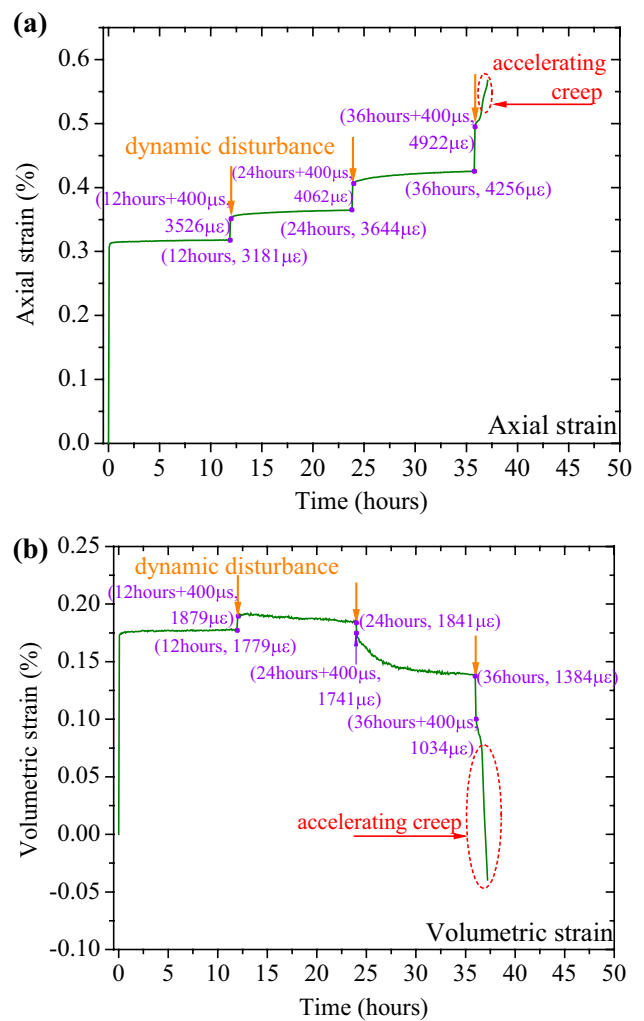


Fig. 10 Strain–time curves during the creep-impact experiment under creep stress of 19.86 MPa and impact energy of 14.7 J: **a** axial strain; **b** volumetric strain. The time for applying dynamic disturbances is indicated. The axial strain and volumetric strain before and after the dynamic disturbances and the onset of accelerating creep are indicated

failed, with a sharper decrease of volumetric strain after the third dynamic disturbance. The dynamic disturbance changed the deformation pattern and hastened the dilatancy rate of the specimen.

This kind of rock creep disturbed by dynamic impact has a similar characteristic to the creep deformation of an underground opening affected by blasting in mining practices, as shown in Fig. 11. In this regard, there is an instantaneous closure at blasting time, followed by a primary phase of decelerating closure within hours, then a steady-state closure phase until the next blast occurs, and this pattern repeats (Malan 1999).

4.3.2 Influence of the First Impact on the Creep Behavior

To further investigate the deformation of the rock specimen affected by the first dynamic disturbance, plots of the axial strain and volumetric strain against time are shown in Fig. 12. The axial strain (Fig. 12a) showed a sudden increase during the dynamic disturbance and a gradual increase during the creep phase. During the dynamic disturbance phase, the axial strain showed an initial increase and reached the peak value (4445 $\mu\epsilon$) at 221 μs after dynamic disturbance was applied; then, the axial strain decreased to a residual strain of 3526 $\mu\epsilon$. The first dynamic disturbance resulted in an increase in axial strain from 3181 to 3526 $\mu\epsilon$. The axial strain rate measured during the creep deformation phase increased from $7.6e^{-10} \text{ s}^{-1}$ (initial creep) to $1.7e^{-9} \text{ s}^{-1}$ during the steady creep stage.

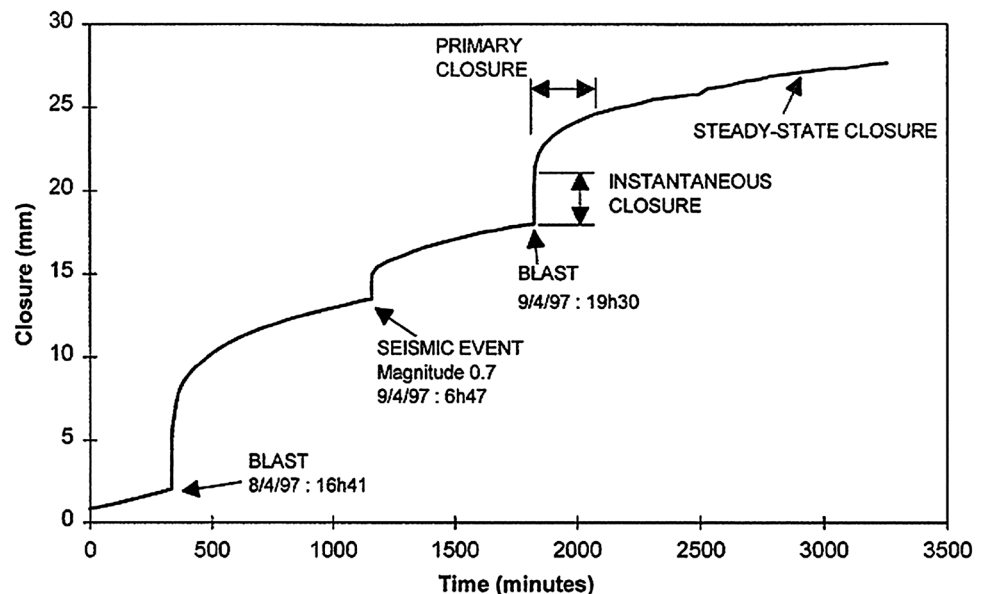
The volumetric strain (Fig. 12b) showed a sudden increase during the dynamic disturbance phase, a gradual increase phase for ~ 59 min, and a quasi-linear decrease phase for the rest of the loading duration during the creep

phase. Similar to the axial strain, the volumetric strain showed a sudden increase (100 $\mu\epsilon$) resulting from the residual strain during dynamic disturbance. During the creep phase afterwards, there was a turning point marking the volumetric strain transition from increase to decrease occurring at ~ 59 min after the first dynamic disturbance. This turning point corresponds to the maximum volumetric strain (Heap et al. 2009a). After the turning point, the volumetric strain rate was $-1.82e^{-9} \text{ s}^{-1}$ during the quasi-linear decreasing phase. The dynamic disturbance not only increased the rate of deformation but also changed the volumetric strain of the rock specimen, which transitioned from an increasing to a decreasing pattern.

4.3.3 Influence of the Third Impact on the Creep Behavior

As shown in Fig. 13, after the third dynamic disturbance, the axial strain increased to 4922 $\mu\epsilon$, correspondingly, the volumetric strain decreased to 1879 $\mu\epsilon$. The rock specimen failed at 76 min after the third dynamic disturbance. Moreover, both the axial strain and the volumetric strain exhibited obvious tri-modal behavior that has been observed in other studies (Lockner 1993; Boukharov et al. 1995; Main 2000; Heap et al. 2011). In the first ~ 9 min, the axial strain and the volumetric strain were characterized by an initially high strain rate that decreased with loading duration to reach a quasi-linear phase. In the quasi-linear phase, an apparent constant-strain rate state lasted for ~ 18 min. Resulting from the third dynamic disturbance, the axial strain rate increased to $4.4e^{-8} \text{ s}^{-1}$. The accelerating creep phase was then entered, characterized by a substantial acceleration in strain rate. This eventually led to the macroscopic failure after ~ 49 min.

Fig. 11 Creep deformation of underground opening affected by blasting in mining practices (Malan 1999)



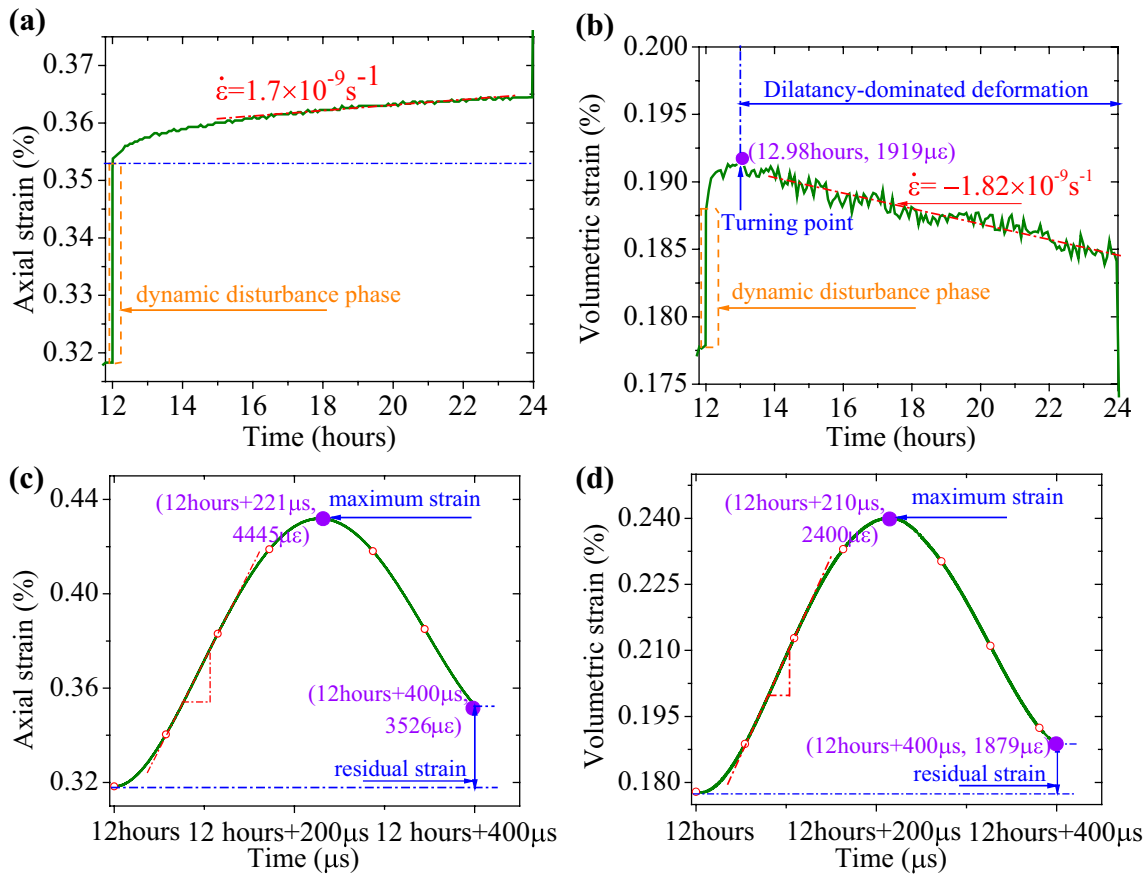


Fig. 12 Strain–time curves affected by the first impact during the creep-disturbance experiment under creep stress of 19.86 MPa and impact energy of 14.7 J: **a** the complete axial strain curve; **b** the complete volumetric strain curve; **c** the axial strain curve during the dynamic disturbance; **d** the volumetric strain curve during the dynamic disturbance. The time for the dynamic disturbance phase,

the turning point (transitioning from compaction-dominated deformation to dilatancy-dominated deformation), the axial strain rate and the volumetric strain rate are indicated in **a**, **b**. The maximum strain and the residual strain during the dynamic disturbance are indicated in **c**, **d**

4.3.4 The Influence of Dynamic Disturbance on AE Characteristics

The AE cumulative energy and AE hit rate during the creep-impact experiment are plotted against time (Fig. 14). The cumulative AE energy exhibited qualitatively similar behavior to the axial strain. Affected by the first dynamic disturbance, the cumulative AE energy consisted of a primary phase and a steady-state phase. The primary phase was characterized by an initially high increase rate that decreased with time to reach the steady-state phase. The AE hit rate showed a high value during the primary phase and remained almost constant during the steady-state phase, although some abrupt high AE hit rates can be observed. This pattern was repeated following the second dynamic disturbance. In comparison with the cumulative AE energy following the first dynamic disturbance, both the AE cumulative energy and AE hit rate following the second dynamic disturbance showed much higher values. Finally, affected

by the third dynamic disturbance, both the cumulative AE energy and AE hit rate increased substantially. The AE cumulative energy exhibited tri-modal behavior until failure, which is consistent with the result of conventional creep (Heap et al. 2009a, 2011). As shown in the zoomed-in view of the AE events after the third dynamic disturbance, most of the cumulative AE energy was released after the onset of accelerated creep. The AE hit rate decreased within the first 0.3 h and then remained at a low level within the next 0.5 h. Finally, the AE hit rate increased rapidly as the failure approached.

4.4 Effect of Creep Stress

The strain curves during the creep-impact experiments under different creep stresses are shown in Fig. 15. Affected by the first dynamic disturbance, under the creep stress of 19.86 MPa and 23.17 MPa, the axial strain curves showed a sudden increase, a primary decelerating phase and a

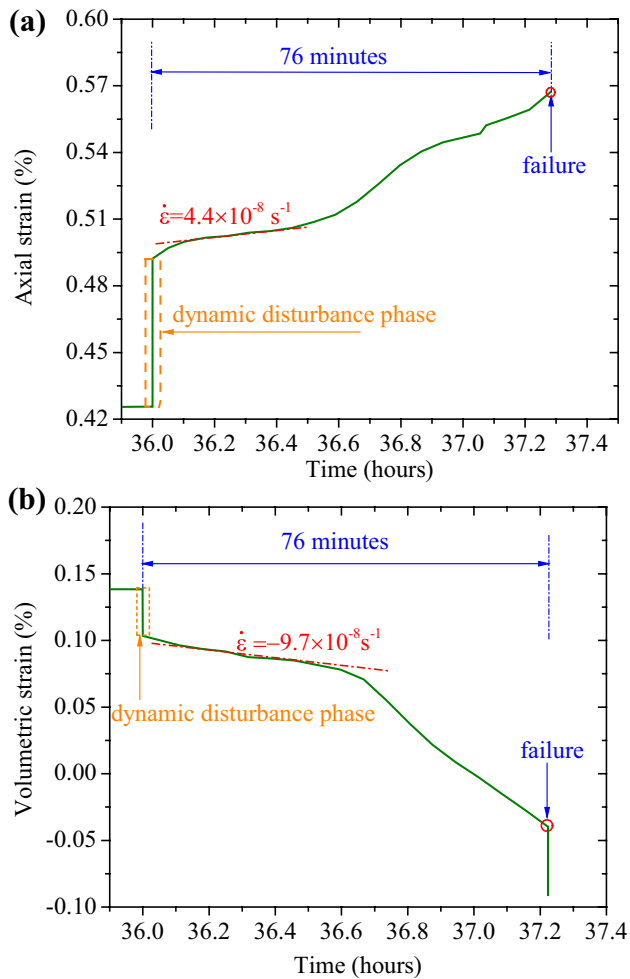


Fig. 13 Strain–time curves affected by the third impact during the creep–impact experiment under creep stress of 19.86 MPa and impact energy of 14.7 J: **a** axial strain curve; **b** volumetric strain curve

steady-state phase. However, the axial strain curve at the creep stress of 26.48 MPa showed a sudden increase and a tri-modal behavior until failure. The volumetric strain curves at creep stresses of 23.17 MPa and 26.48 MPa showed an initial sudden decrease, which is different from the result at 19.86 MPa. Affected by the second dynamic disturbance, the specimen under the creep stress of 23.17 MPa failed immediately. Under the same dynamic disturbance, the specimen failed faster with increasing creep stress.

The relation between the strain rate and the count of dynamic disturbances is shown in Fig. 16. Because the strain rate during the dilatancy state is negative, we chose the absolute value of volumetric strain to aid comparison. Both the axial strain rate and the absolute volumetric strain rate increased obviously with increasing dynamic disturbances. Meanwhile, under the same count of dynamic disturbances, the axial strain rate and the absolute volumetric

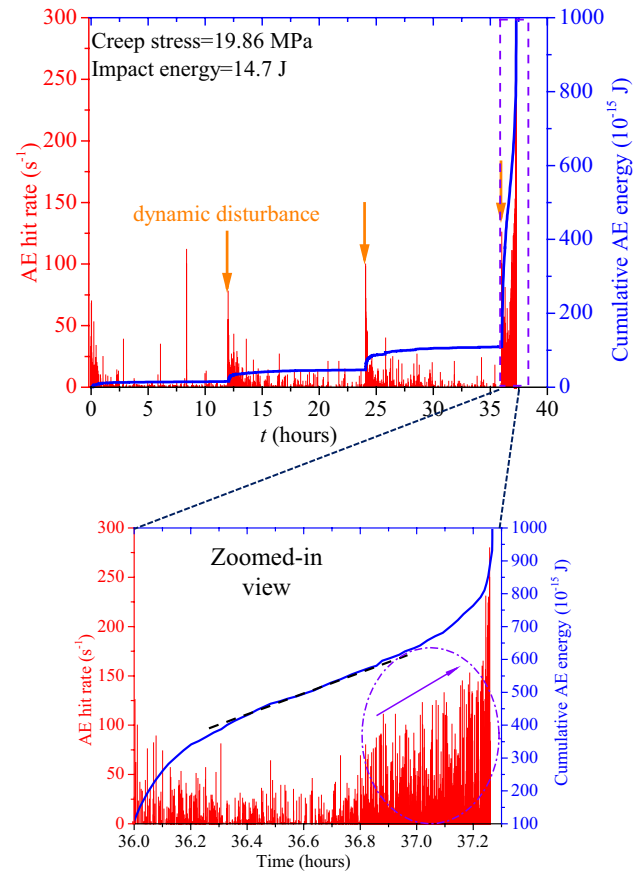


Fig. 14 AE behavior during the creep–disturbance experiment under creep stress of 19.86 MPa and impact energy of 14.7 J. A zoomed-in view of the AE behavior after the third impact is shown. **a** Creep stress = 23.17 MPa. **b** Creep stress = 26.48 MPa

strain rate showed higher values under the higher creep stress. It means that the rock creep deformation is more sensitive to dynamic disturbance under the higher creep stress.

The AE behaviors under different creep stresses are shown in Fig. 17. Affected by the first dynamic disturbance, both the AE cumulative energy curves and the AE hit rates obtained in the test with the creep stress of 19.86 MPa and 23.17 MPa showed a primary decelerating phase and a steady-state phase. However, under the creep stress of 26.48 MPa, both the AE cumulative energy curve and the AE hit rate showed tri-modal behavior, because the strain energy and damage accumulated in the rock specimen are sufficient to induce the accelerating creep of rock specimens under the triggering by dynamic disturbance. As shown in Fig. 17c, in response to the first dynamic disturbance, the AE energy rate showed a higher value with the increase of creep stress, which resulted from more microcracks having been generated under higher creep stress.

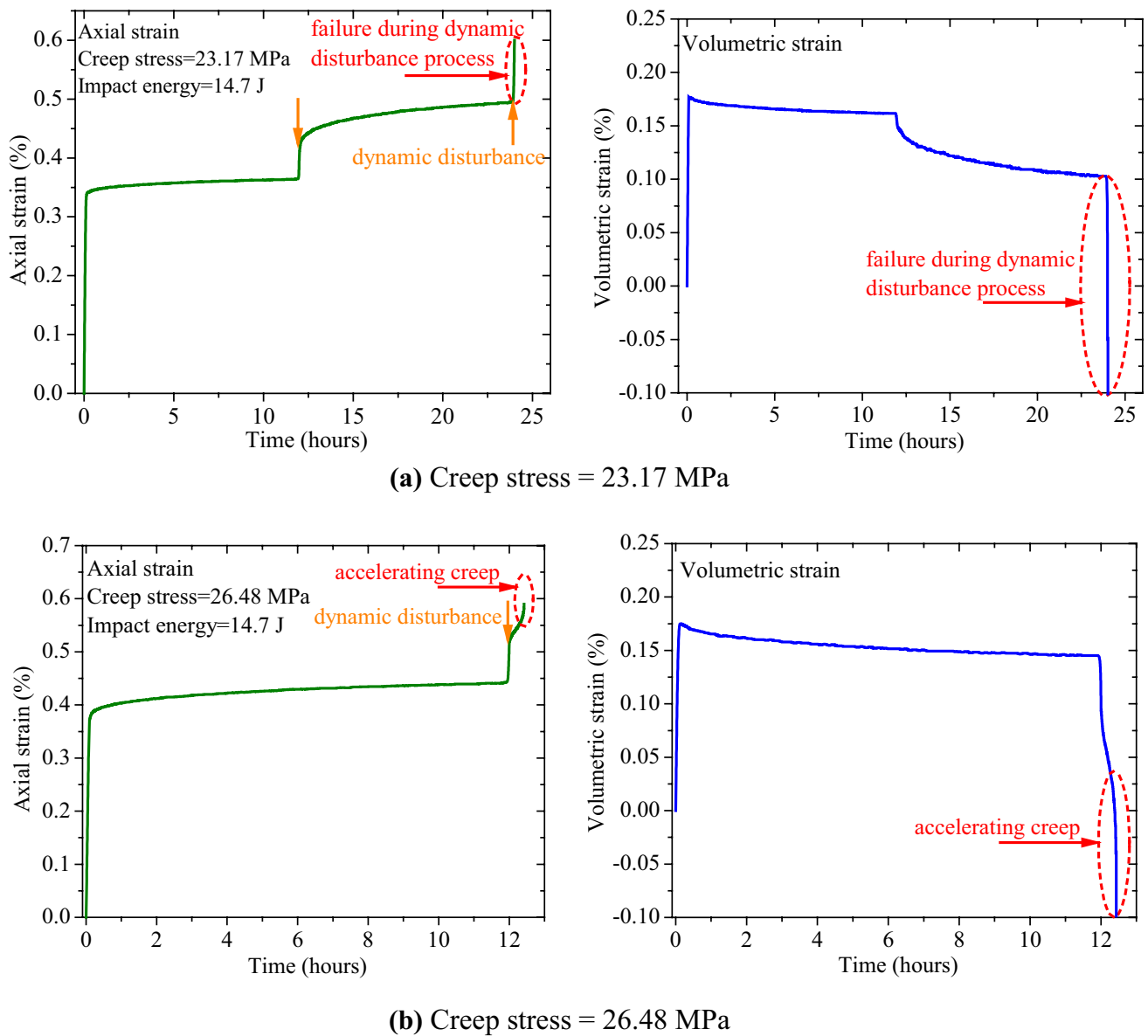


Fig. 15 Strain–time curves during the creep-impact experiment with different creep stresses. The time for applying dynamic disturbances is indicated

4.5 Effect of Impact Energy

The strain and strain rate during the creep-impact experiments of rock specimens with different impact energies are shown in Fig. 18. The time-to-failure shortened from 37.26 h to 33.68 h and to 28.20 h as the impact energy increased from 14.7 J to 19.6 J and to 24.5 J, respectively. Affected by the first dynamic disturbance, all of the axial strain curves showed a sudden increase, a primary decelerating phase and a steady-state phase. Under the influence of the second dynamic disturbances with impact energies of 19.6 J and 24.5 J, rock specimens failed within

12 h along with accelerating creep. It is noted that higher impact energy resulted in faster failure of rock specimens.

The curves between the strain rate and the count of dynamic disturbances are shown in Fig. 18c. The axial strain rate increased obviously with the increasing count of dynamic disturbances. Under the same count of dynamic disturbances, the axial strain rate increased with the input impact energy. Following the first dynamic disturbance, as the impact energy increased from 14.7 J to 19.6 J and to 24.5 J, the axial strain rate increased from $1.7 \times 10^{-9} \text{ s}^{-1}$ to $2.1 \times 10^{-9} \text{ s}^{-1}$ and to $3 \times 10^{-9} \text{ s}^{-1}$, respectively. It means that the

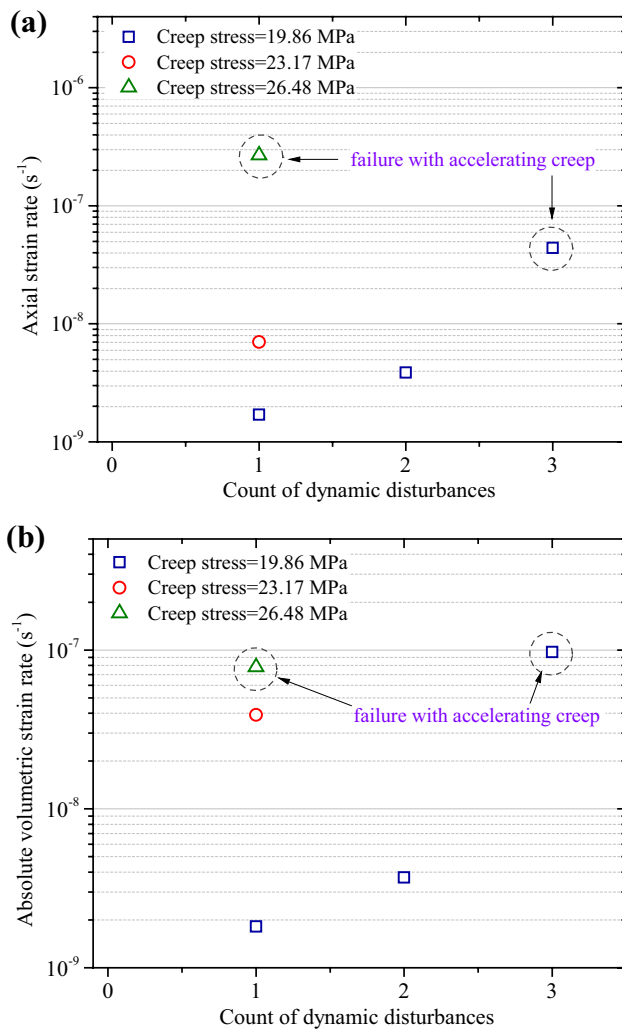


Fig. 16 Strain rate during the creep-impact experiment with different creep stresses: **a** axial strain rate, **b** absolute volumetric strain rate

higher impact energy resulted in a higher axial deformation rate.

The AE behaviors during the creep-impact experiments with different impact energies are shown in Fig. 19. Affected by the first dynamic disturbance, both the cumulative AE energy and AE hit rate consisted of a primary phase and a steady-state phase. Unlike the result with the impact energy of 14.7 J, both the cumulative AE energy under the impact energies of 19.6 J and 24.5 J showed tri-modal behavior affected by the second dynamic disturbance, which is consistent with the behavior of the strain curve. As shown in Fig. 19c, all of the AE energy rates exhibited an increase with the increasing count of dynamic disturbances. Following the first dynamic disturbance, as the impact energy increased from 14.7 J to 19.6 J and to 24.5 J, the AE energy rate increased from $15e^{-20}$ J s⁻¹ to $20e^{-20}$ J s⁻¹ and to $28.5e^{-20}$ J s⁻¹, respectively. Under the same count of

dynamic disturbance, the AE energy rate increased with the increasing impact energy, which means that more microcracks were generated under the higher impact energy.

4.6 The Failure Pattern

The failure patterns of rock specimens during creep-impact experiments with different creep stresses and impact energies are shown in Fig. 20. The failed specimens included two main parts and some small spalling debris. All of the final failure patterns looked similar to a shear dominant mode. Under different creep stresses, the angles of the shear plane were approximately 60°, which indicated that the creep stress had little effect on the final failure pattern. The larger the impact energy was, the smaller the residual parts were. Obvious cones were generated as the impact energy increased to 19.6 J and 24.5 J. The angles of the shear plane to the horizon were 61°, 50° and 42° under impact energies of 14.7 J, 19.6 J and 24.5 J, respectively, which indicated that the impact energy did not substantially alter the final failure pattern. In general, the specimen is more fragmented under the higher creep stress and the larger impact energy.

5 Discussion

Affected by dynamic disturbances, the original microcracks may propagate and new microcracks may initiate (Aben et al. 2016), which led to the sudden change of strain. This kind of initiation and propagation of microcracks can be generally characterized as damage in the framework of continuum mechanics, which can also be quantified by the AE data. In this regard, the increase in axial strain rate is at least partially expected, since the rate of rock damage would increase following the dynamic disturbances, although the creep stress level was kept constant after an interval of 20,000 μ s. This has been supported by the results of AE activity. Under the same creep stress, more damage was achieved by dynamic disturbance with higher impact energy. Then, there is a higher initial damage level for the next phase of creep. Brantut et al. (2013) reported that a material with a higher level of initial defects will creep faster. They attributed this to the increase of number and growth rate of cracks subjected to subcritical crack growth. Thus, faster creep is expected as the result of the dynamic disturbance with higher impact energy.

There are two different kinds of failure conditions: failure along with accelerating creep and failure during dynamic disturbance. If the accumulated damage reaches a high level before dynamic disturbance, the rock specimen will fail during the dynamic disturbance although the impact energy is low, such as the experiment under

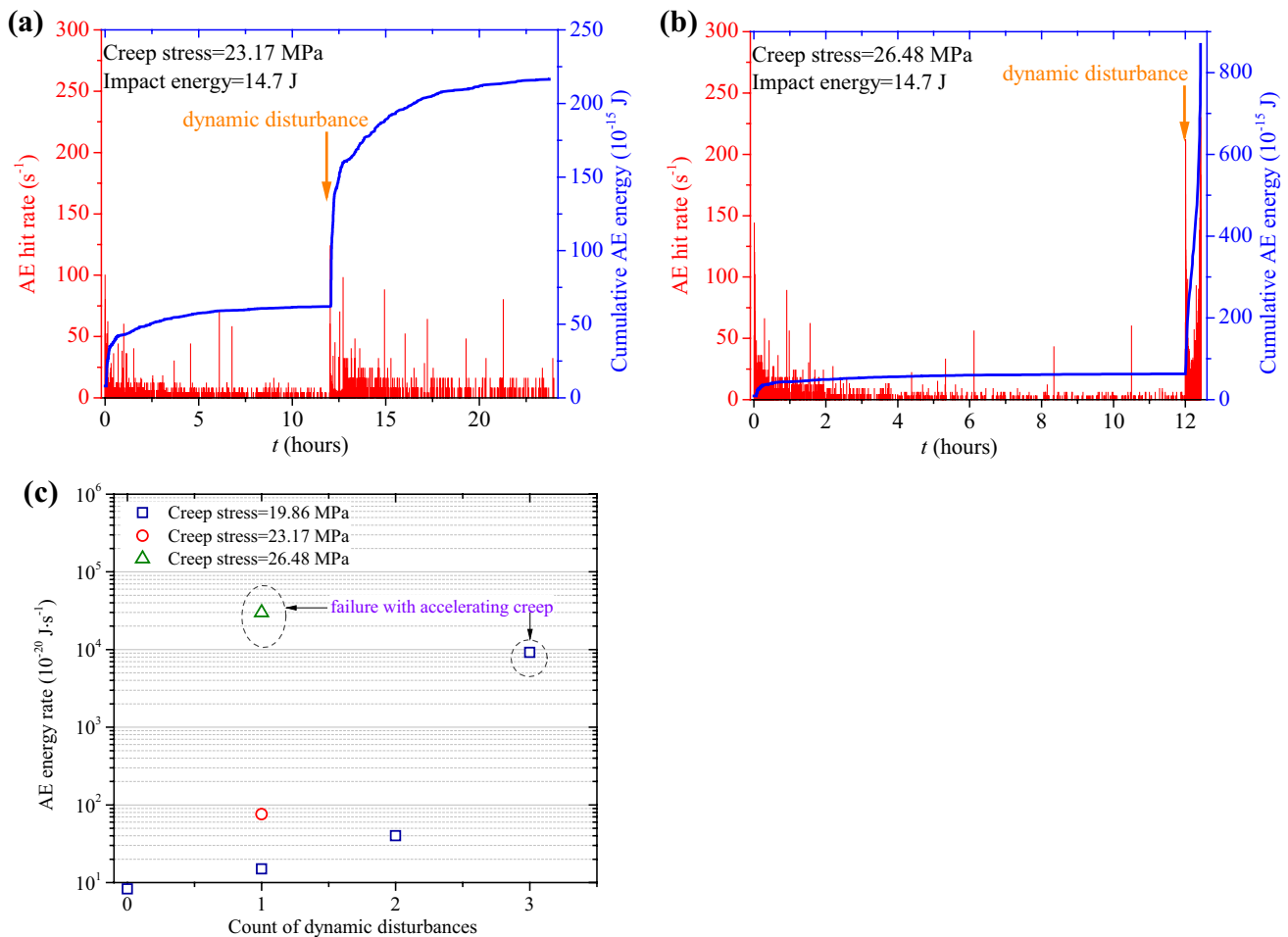


Fig. 17 AE behaviors during the creep-impact experiment with different creep stresses: **a, b** AE cumulative energy curves, **c** AE energy rate

the creep stress of 23.17 MPa and the impact energy of 14.7 J. It has been accepted that a critical level of damage is required to initiate the onset of acceleration to failure (Griggs 1939; Heap et al. 2009a, b, 2011). Likewise, a critical volumetric strain was required for the commencement of tertiary creep (Kranz and Scholz 1977; Baud and Meredith 1997). Because of the damage induced by the dynamic disturbance, the rock creep during the next 12 h will exhibit a higher deformation rate. Accelerating creep will initiate as the critical level of damage is achieved and the rock specimen fails along with the accelerating creep after a dynamic disturbance. This may explain why rock failure instability does not always occur at blasting time, but occurs when there is no external influence that could account for changes in the stress distribution. Thus, the two kinds of failure types are attributed to the accumulation of strain energy and damage in rock specimens under the combined contribution of creep stress and dynamic disturbance.

6 Conclusion

The effects of creep stress and impact energy on the creep behavior of sandstone during creep-impact experiments were investigated. The following conclusions can be drawn:

1. Dynamic disturbance hastened the failure of rock specimens under creep stress. The combination of creep stress and dynamic disturbance resulted in two failure conditions: failure along with accelerating creep and failure during dynamic disturbance. The failures of the rock specimens were mostly in the shear mode. The failed specimen included two main parts and some small spalling debris.
2. Dynamic disturbance not only increased the axial strain rate but also promoted the dilatancy of the rock specimen. For the dynamic disturbance not followed by instantaneous failure, the axial strain curve consisted of an instantaneous response at the dynamic disturbance time, followed by a primary phase of decelerating creep

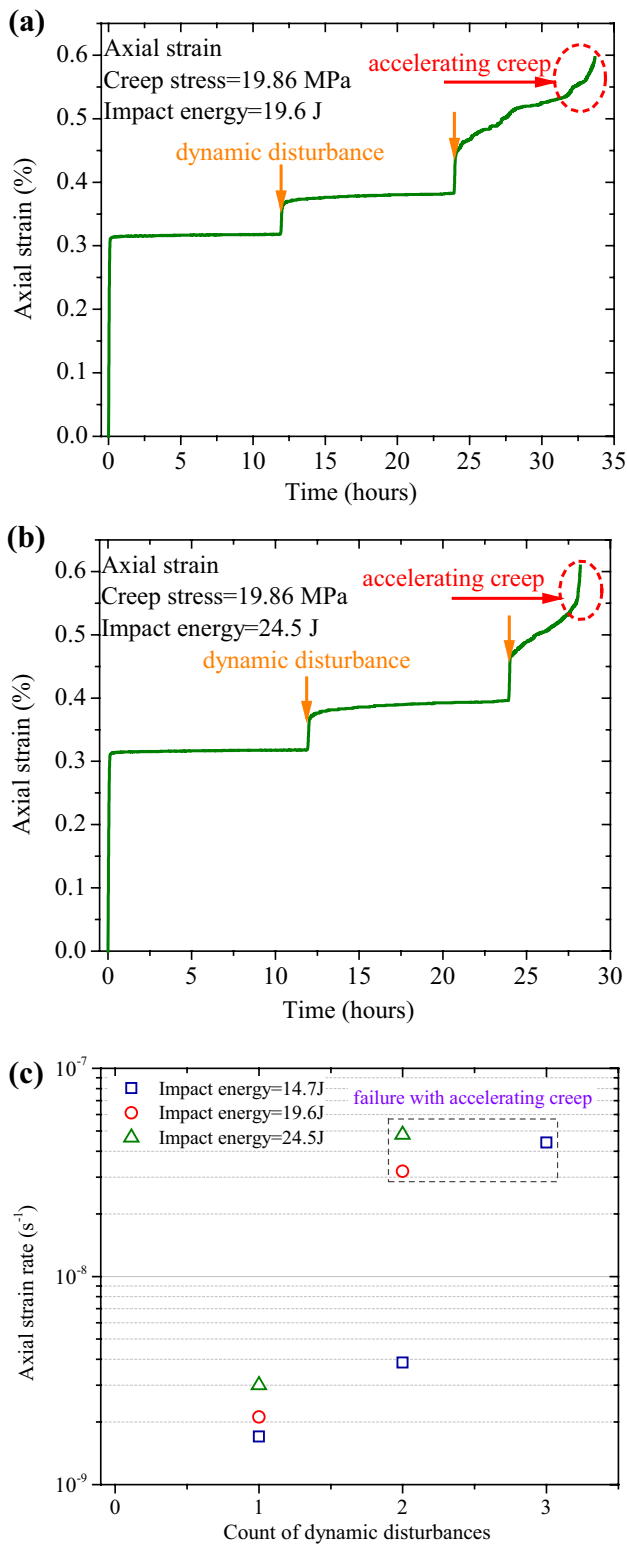


Fig. 18 Strain and strain rate of the rock specimens during the creep-impact experiment with different impact energies: **a** Strain curve at impact energy of 19.6 J, **b** strain curve at impact energy 24.5 J, **c** strain rates

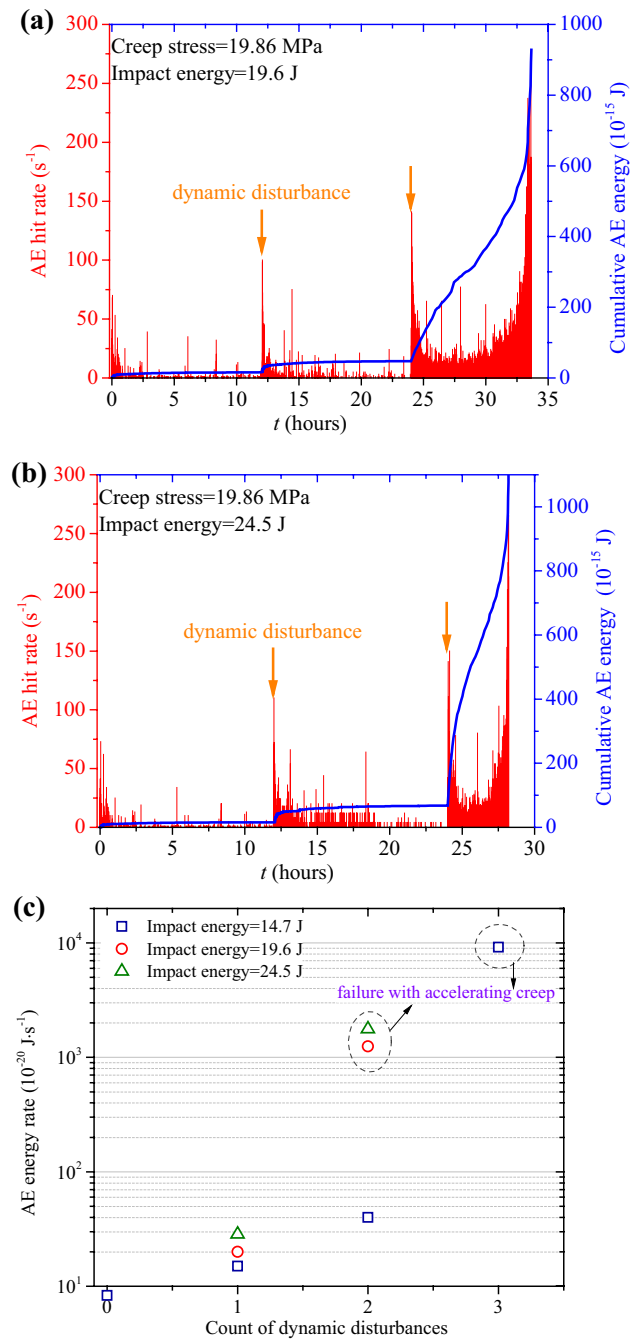


Fig. 19 AE behaviors during the creep-disturbance experiment with different impact energies: **a** AE behaviors with impact energy of 19.6 J, **b** AE behaviors with impact energy of 24.5 J, **c** AE energy rate

and a steady-state phase. This pattern was repeated after the next dynamic disturbance until the last dynamic disturbance that led to the final failure. AE accumulative energy exhibited a similar behavior to the axial strain, which indicates that dynamic disturbance induced further damage in the rock specimen. This kind of effect of dynamic disturbance on the rock creep is consistent with


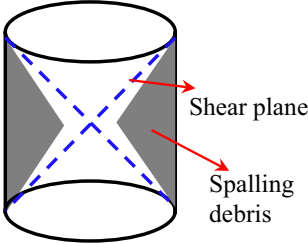
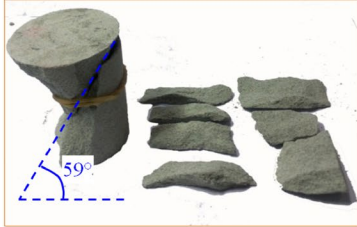

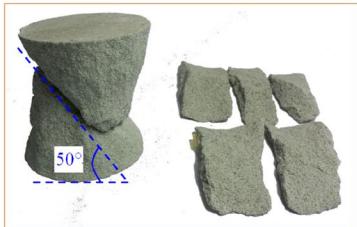

Creep stress (MPa)	Impact energy (J)	Failure pattern	Sketch of failure pattern
19.86	14.7		
23.17	14.7		
26.48	14.7		
19.86	19.6		
19.86	24.5		

Fig. 20 Summary of the failure pattern of the rock specimens during creep-impact experiments

the observation of creep deformation in mining practices monitored during and after blasting (Malan et al. 1997; Malan 1999).

- The creep behavior of sandstone is sensitive to dynamic disturbance under the higher creep stress. Under a dynamic disturbance with impact energy of 14.7 J, creep stresses of 19.86 MPa, 23.17 MPa and 26.48 MPa

resulted in times-to-failure of 37.26 h, 24 h and 12.42 h, respectively, indicating the faster failure of rock under higher creep stress. Under the same dynamic disturbance, the specimen failed faster and axial strain rate, absolute volumetric strain rate and AE energy rate increased under increasing creep stress. It means that

the sensitivity of creep behavior to dynamic disturbance increased with increasing creep stress.

4. Under the same creep stress, a dynamic disturbance with a higher impact energy resulted in shorter failure time and larger axial strain rate, high absolute volumetric strain rate and high AE energy rate. For example, under a creep stress of 19.86 MPa, dynamic disturbances with impact energies of 14.7 J, 19.6 J and 24.5 J resulted in times-to-failure of 37.26 h, 33.68 h and 28.20 h, respectively. Following the first dynamic disturbance, the axial strain rate increased from $1.7e^{-9} s^{-1}$ to $2.1e^{-9} s^{-1}$ and to $3e^{-9} s^{-1}$ as the impact energy increased from 14.7 J to 19.6 J and to 24.5 J, respectively. Both the absolute volumetric strain rate and AE energy rate showed the same tendency, increasing with the impact energy.
5. In general, the specimen is considerably more fragmented under the higher creep stress and the larger impact energy. All of the final failure patterns looked similar to a shear dominant mode, and the creep stress and impact energy had little effect on the final failure pattern.

Acknowledgements This work is funded by the National Key Research and Development Program of China (Grant No. 2016YFC0801607), the National Science Foundation of China (Grant Nos. 51525402, 51874069 and 51761135102), and the Fundamental Research Funds for the Central Universities of China (Grant Nos. N170108028 and N160103005). These supports are gratefully acknowledged.

References

- Aben FM, Doan ML, Mitchell TM, Toussaint R, Reuschlé T, Fondriest M, Gratier JP, Renard F (2016) Dynamic fracturing by successive coseismic loadings leads to pulverization in active fault zones. *J Geophys Res-Sol Ea* 121(4):2338–2360
- Anderson OL, Grew PC (1977) Stress corrosion theory of crack propagation with applications to geophysics. *Rev Geophys* 15(1):69–84
- Atkinson BK (1984) Subcritical crack growth in geological materials. *J Geophys Res-Sol Ea* 89(B6):4077–4114
- Atkinson BK, Meredith PG (1987) The theory of subcritical crack growth with applications to minerals and rocks. *Fract Mech Rock*: 111–166
- Aydan Ö, Ito T, Özbay U, Kwasniewski M, Shariar K, Okuno T, Özgenoğlu A, Malan DF, Okada T (2014) ISRM suggested methods for determining the creep characteristics of rock. *Rock Mech Rock Eng* 47(1):275–290
- Baud P, Meredith PG (1997) Damage accumulation during triaxial creep of Darley Dale sandstone from pore volumetry and acoustic emission. *Int J Rock Mech Min* 34(3–4): 24:e21–e24. (e10)
- Boukharov GN, Chanda MW, Boukharov NG (1995) The three processes of brittle crystalline rock creep. *Int J Rock Mech Min* 32(4):325–335
- Brace WF, Paulding BW, Scholz C (1966) Dilatancy in the fracture of crystalline rocks. *J Geophys Res* 71(16):3939–3953
- Brantut N, Baud P, Heap MJ, Meredith PG (2012) Micromechanics of brittle creep in rocks. *J Geophys Res-Sol Ea* 117(B8):1133–1172
- Brantut N, Heap MJ, Meredith PG, Baud P (2013) Time-dependent cracking and brittle creep in crustal rocks: a review. *J Struct Geol* 52(5):17–43
- Brantut N, Heap MJ, Baud P, Meredith PG (2014a) Rate- and strain-dependent brittle deformation of Rocks. *J Geophys Res-Sol Ea* 119(3):1818–1836
- Brantut N, Heap MJ, Baud P, Meredith PG (2014b) Mechanisms of time-dependent deformation in porous limestone. *J Geophys Res-Sol Ea* 119(7):5444–5463
- Chen L, Wang CP, Liu JF, Liu YM, Liu J, Su R, Wang J (2014) A damage-mechanism-based creep model considering temperature effect in granite. *Mech Res Commun* 56(2):76–82
- Chen L, Liu J, Wang C (2015) Experimental investigation on the creep behavior of Beishan granite under different temperature and stress conditions. *Eur J Environ Civ En* 19(sup1):43–53
- Costin LS (1987) Time-dependent deformation and failure. *Fract Mech Rock* 167–215
- Dawson PR, Munson DE (1983) Numerical simulation of creep deformations around a room in a deep potash mine. *Int J Rock Mech Min* 20(1):33–42
- Fu ZL, Guo H, Gao YF (2008) Creep damage characteristics of soft rock under disturbance loads. *J Earth Sci* 19(3):292–297
- Fujii Y, Kiyama T, Ishijima Y, Kodama J (1999) Circumferential strain behavior during creep tests of brittle rocks. *Int J Rock Mech Min* 36(3):323–337
- Griggs D (1939) Creep of Rocks. *J Geol* 47(3):225–251
- Hansen FD (1978) Quasi-static strength and creep deformational characteristics of bedded salt from the Carey mine near Lyons, Kansas. Technical Memorandum Report RSI-0067, Office of Waste Isolation, Oak Ridge, Tennessee
- Heap MJ, Baud P, Meredith PG, Bell AF, Main IG (2009a) Time-dependent brittle creep in Darley Dale sandstone. *J Geophys Res-Atmos* 114(B7):4288–4309
- Heap MJ, Baud P, Meredith PG (2009b) Influence of temperature on brittle creep in sandstones. *Geophys Res Lett* 36(19):308–308
- Heap MJ, Baud P, Meredith PG, Vinciguerra S, Bell AF, Main IG (2011) Brittle creep in basalt and its application to time-dependent volcano deformation. *Earth Planet Sc Lett* 307(1–2):71–82
- Kranz RL (1980) The effects of confining pressure and stress difference on static fatigue of granite. *J Geophys Res-Sol Ea* 85(B4):1854–1866
- Kranz RL, Scholz CH (1977) Critical dilatant volume of rocks at the onset of Tertiary creep. *J Geophys Res* 82(30):4893–4898
- Kranz RL, Harris WJ, Carter NL (1982) Static fatigue of granite at 200 °C. *Geophys Res Lett* 9(1):1–4
- Li XB, Zhou ZL, Lok TS, Hong L, Yin T (2008) Innovative testing technique of rock subjected to coupled static and dynamic loads. *Int J Rock Mech Min* 45(5):739–748
- Li SH, Zhu WC, Niu LL, Dai F (2017) Constant strain rate uniaxial compression of green sandstone during SHPB tests driven by Pendulum Hammer. *Shock Vib* 2017(1):1–12
- Li SH, Zhu WC, Niu LL, Yu M, Chen CF (2018) Dynamic characteristics of green sandstone subjected to repetitive impact loading: phenomena and mechanisms. *Rock Mech Rock Eng* 2018(4):1–16
- Lockner D (1993) Room temperature creep in saturated granite. *J Geophys Res-Atmos* 98(B1):475–487
- Lockner D, Byerlee J (1977) Acoustic emission and creep in rock at high confining pressure and differential stress. *B Seismol Soc Am* 67(2):247–258
- Ma L, Daemen JJK (2006) An experimental study on creep of welded tuff. *Int J Rock Mech Min* 43(2):282–291
- Main IG (2000) A damage mechanics model for power-law creep and earthquake aftershock and foreshock sequences. *Geophys J Roy Astr S* 142(1):151–161
- Malan DF (1999) Time-dependent behaviour of deep level tabular excavations in hard rock. *Rock Mech Rock Eng* 32(2):123–155

- Malan DF, Vogler UW, Drescher K (1997) Time-dependent behaviour of hard rock in deep level gold mines. *J S Afr I Min Metall* 97(3):135–147
- Mansurov VA (2001) Prediction of rockbursts by analysis of induced seismicity data. *Int J Rock Mech Min* 38(6):893–901
- Molladavoodi H, Mortazavi A (2011) A damage-based numerical analysis of brittle rocks failure mechanism. *Finite Elem Anal Des* 47(9):991–1003
- Mortazavi A, Molladavoodi H (2012) A numerical investigation of brittle rock damage model in deep underground openings. *Eng Fract Mech* 90:101–120
- Ngwenya BT, Main IG, Elphick SC, Crawford BR, Smart BGD (2001) A constitutive law for low-temperature creep of water-saturated sandstones. *J Geophys Res-Sol Ea* 106(B10):21811–21826
- Nicolas A, Fortin J, Regnet JB, Verberne BA, Plümper O, Dimanov A, Spiers CJ, Guéguen Y (2017) Brittle and semi-brittle creep of tavel limestone deformed at room temperature. *J Geophys Res-Sol Ea* 122(6):4436–4459
- Niemeijer AR, Spiers CJ, Bos B (2002) Compaction creep of quartz sand at 400–600 °C: experimental evidence for dissolution-controlled pressure solution. *Earth Planet Sc Lett* 195(3–4):261–275
- Obert L (1965) Creep in model pillars. Bureau of Mines, College Park, MD, USA
- Sone H, Zoback MD (2014) Time-dependent deformation of shale gas reservoir rocks and its long-term effect on the in situ state of stress. *Int J Rock Mech Min* 69(3):120–132
- Urai JL, Spiers CJ, Zwart HJ, Lister GS (1986) Weakening of rock salt by water during long-term creep. *Nature* 324(6097):554–557
- Wang X, Huang R (1998) Analysis of the influence of the dynamic disturbance on rock burst. *J Mountain Res* 16(3):188–192
- Xia KW, Yao W (2015) Dynamic rock tests using split Hopkinson (Kolsky) bar system—a review. *J Rock Mech Geotech* 7(1):27–59
- Xu T, Zhou GL, Heap MJ, Zhu WC, Chen CF, Baud P (2017) The Influence of temperature on time-dependent deformation and failure in granite: a mesoscale modeling approach. *Rock Mech Rock Eng* 50(9):2345–2364
- Ye GL, Nishimura T, Zhang F (2015) Experimental study on shear and creep behaviour of green tuff at high temperatures. *Int J Rock Mech Min* 79:19–28
- Yoshida H, Horii H (1992) A micromechanics-based model for creep behavior of rock. *Appl Mech Rev* 45(8):294–303
- Zhang QB, Zhao J (2014) A review of dynamic experimental techniques and mechanical behaviour of rock materials. *Rock Mech Rock Eng* 47(4):1411–1478
- Zhang H, Wang Z, Zheng Y, Duan P, Ding S (2012) Study on tri-axial creep experiment and constitutive relation of different rock salt. *Safety Sci* 50(4):801–805
- Zhu WC, Li ZH, Zhu L, Tang CA (2010) Numerical simulation on rockburst of underground opening triggered by dynamic disturbance. *Tunn Undergr Sp Tech* 25(5):587–599
- Zhu WC, Niu LL, Li SH, Xu ZH (2015) Dynamic brazilian test of rock under intermediate strain rate: Pendulum Hammer-Driven SHPB test and numerical simulation. *Rock Mech Rock Eng* 48(5):1867–1881
- Zhu WC, Li S, Niu LL, Liu K, Xu T (2016) Experimental and numerical study on stress relaxation of sandstones disturbed by dynamic loading. *Rock Mech Rock Eng* 49(10):3963–3982
- Whyatt JK, Blake W, Williams TJ, White BG (2002) 60 years of rock-bursting in the Coeur D’alene district of northern Idaho. USA: lessons learned and remaining issues. In: Proceedings of the 109th Annual Exhibit and Meeting, Society for Mining, Metallurgy, and Exploration, February 25–27, 2002, Phoenix, AZ. Preprint 02-164. Society for Mining, Metallurgy, and Exploration, Inc., Littleton, CO, pp 1–10

Publisher’s Note Springer Nature remains neutral with regard to jurisdictional claims in published maps and institutional affiliations.